EXPERIMENTAL CHARACTERIZATION OF MOISTURE TRANSPORT IN BRICK MASONRY WITH NATURAL HYDRAULIC LIME MORTAR

R. Ramirez[a,*], B. Ghiassi[b], P. Pineda[c], P.B. Lourenço[a]

[a] *University of Minho, Institute for Sustainability and Innovation in Structural Engineering (ISISE), Department of Civil Engineering, Campus de Azurém s/n, 4800-085 Guimarães, Portugal*

[b] *Centre for Structural Engineering Design and Informatics (CSEI), Faculty of Engineering, University of Nottingham, University Park, NG7 2RD Nottingham, United Kingdom*

[c] *School of Architecture, Department of Building Structures and Geotechnical Engineering, University of Seville, Avda. Reina Mercedes 2, 41012 Seville, Spain*

* *Corresponding author. Mail: Institute for Sustainability and Innovation in Civil Engineering, University of Minho, Campus de Azurém, s/n, 4800-058 Guimarães, Portugal. E-mail:* rafael.alvarezdelara@gmail.com. Telephone: +351 910905513

ABSTRACT

This article presents an experimental study on the hygric performance of brick masonry with a special focus on the hydraulic characterization of the brick-mortar interface. The hygric behavior was studied at the level of the constituent materials as well as at the composite scale. An extruded fired-clay brick and two types of mortar –Portland cement mortar and natural hydraulic lime mortar– were chosen as target materials. The hygric properties were determined following prescribed experimental procedures. The experimental program included vacuum saturation tests, static gravimetric tests for adsorption/desorption isotherms, dry/wet cup tests, capillary absorption tests, and isothermal one-dimensional drying. The results allowed for a comprehensive identification of the main hygric features of the target materials. Fired-clay brick and lime mortar revealed low hygroscopicity and a strong capillary-active behavior with negligible hysteresis, whereas cement mortar showed activity in both hygroscopic and capillary ranges with a distinct moisture storage hysteresis. Different curing conditions led to dissimilar properties between the lime mortar prepared in molds and the same mortar cured in masonry bed joints. Water absorption in fired-clay bricks showed a marked anisotropic behavior, likely derived from the extrusion process. The existence of an imperfect hydraulic contact at the brick-mortar interface was demonstrated for water absorption. Conversely, the interfacial effect on drying kinetics was not evident.

Keywords: Masonry; moisture transport; hygric characterization; porous building material; multi-layered

material; brick-mortar interface

1. INTRODUCTION

Masonry has been traditionally used as the main construction material in historical structures all around the world. Nowadays, brickwork is still commonly used in veneer walls within contemporary frame structures. Due to their enveloping nature, masonry walls play a major role in the overall energy efficiency of buildings and control of indoor conditions [1–3]. Moreover, the external walls are usually exposed to environmental actions, such as solar radiation, wind-driven rain, moisture condensation and rising damp, among others. Such environmental exposure consequently produces a degradation in each constituent material as well as in masonry as a whole [4,5]. From a durability point of view, moisture-related processes are of special interest since they may lead to significant damage, e.g. cracking due to hygric swelling and contraction, spalling caused by freeze-thaw cycles and (crypto)efflorescence due to salt crystallization [6,7]. Hence, prevention and reparation of moisture-related damage in masonry require a thorough understanding of its hygric behaviour.

Due to the importance of moisture phenomena, different theoretical models and numerical tools have been developed to account for moisture transport in porous media [8–10]. Regardless of the chosen approach, a series of material parameters is always necessary to describe the hygric behavior of a given porous medium. This basic set of material data encompasses both moisture storage and moisture transport properties including both liquid and gas (vapor) phases. In the hygroscopic range (0-95% relative humidity, RH), water vapor plays the key role and moisture transport occurs mainly through vapor diffusion. In the over-hygroscopic or capillary range (95-100% RH), liquid transport by capillarity dominates the moisture transfer. A set of basic experiments and derived material properties for the characterization of a porous material over the entire moisture range was defined by Scheffler [11]. It includes general properties, such as bulk density and open porosity, moisture storage capacity, vapor diffusion properties, and liquid transport properties, such as liquid water diffusivity or permeability, which may be derived from water absorption experiments and drying tests.

Several round-robin initiatives have been launched to define and collect hygric properties of commonly used porous building materials, e.g. IEA Annex 24 [12] and EC HAMSTAD [13]. Nevertheless, considerably large variations were reported for some materials, including certain types of masonry units and mortar mixes. The reason behind such deviations is manyfold. On one hand, ceramic products and mortars are hardly free of intrinsic variability and inhomogeneities. Even industrially produced bricks can

have highly variable properties depending on the raw materials and the forming and firing methods [14,15]. Similarly, mortar mixes are in-situ prepared materials, and their final properties depend on the type and proportion of components as well as on the curing conditions. Moreover, the registered variation present in the literature may also come from the testing process itself, e.g. lack of a unified experimental setup, operator expertise and familiarity with the procedure, neglected factors such as temperature, etc. While intrinsic material variability can hardly be overcome univocally, the standardization and consistent implementation of experimental procedures is still a work-in-progress to minimize testing errors. Indeed, some works have focused on repeatability and reproducibility of the testing methods to determine hygric properties [16–18]. Shared conclusions were the importance of applying a unified approach, the value of providing a detailed report of testing conditions and procedures, and the need for a revision of the current vapor permeability testing methods. In this context, a thorough material characterization contributes to improving the quality of available material databases as well as increasing our confidence in the reported values and test protocols.

Numerous works in the literature have documented the hygric properties of clay brick as a porous building material, e.g. [11–13,19]. However, given the high intrinsic variability previously mentioned, the extrapolation of literature data to specific real case scenarios is not always straightforward. Moreover, most databases assume isotropic properties and very few references point at an anisotropic behavior, which has been nonetheless demonstrated for both molded [20] and extruded [21] bricks.

The most common mortars used in masonry structures are lime- and cement-based mixes [22]. Lime mortars are more frequently found in historical constructions. However, most hygric characterization studies have focused on cement-based mixes. Similarly, the available studies on brick masonry are mostly concern with cement-based or blended lime-cement mortars, and few cases tackle the combination of brick and lime-based mixes, e.g. [23–26].

Several authors have dealt with moisture transport in multi-layered materials such as masonry [27–35]. The existing literature comprises experimental, analytic, and numerical works, which account for the interfacial effects from different viewpoints. Most of the research is focused on liquid water uptake whereas drying has been scarcely studied [27]. Wilson *et al*. [28,29] studied sorption phenomena in multi-layered building materials, namely plaster and plaster/sand mixtures. The authors used analytic expressions based on the sharp front model and assumed perfect hydraulic contact at the interface. Their experimental studies showed

an overall good match with the analytic solutions, but some deviations were identified. The differences were explained as a consequence of the wet sharp front simplification. Hall and Hoff [30] later extended this approach to account for imperfect hydraulic contact cases and introduced the interfacial resistance as an additional cause to explain the observed discrepancies.

Considering the possible causes that may lead to the existence of a hydraulic resistance at the brick-mortar interface, a commonly accepted explanation is related to the curing conditions of the bedding mortar between bricks [27,31]. During application, bricks absorb water from the fresh mortar, which leads to a drop in the water-binder ratio of the mixture. Furthermore, water extraction from the mortar is also connected to the transport of fine binder particles towards the interface and a stratification of the mortar across the joint thickness. Consequently, one would expect a denser, more compact mortar at the interface. However, this is not always the case since a more porous mortar near the interface may be equally found in real scenarios. To account for this fact, Groot and Larbi [32] hypothesized a reversed water flow from brick to mortar after compaction and initial hydration of the mortar, with subsequent impact on the interface development. Overall, the quality of brick-mortar interfaces seems to be highly dependent on the curing history of the mortar. Derluyn *et al*. [33] and Janssen *et al*. [34] studied the absorption behavior of brick-cement masonry composites with different interfacial configurations, namely perfect hydraulic contact (kaolin layer), and wet- and dry-cured specimens. Their studies confirmed that the interfacial effects were proportional to the water extraction from the mortar during curing. Further causes for the existence of a hydraulic resistance at the brick-mortar interface can be the presence of air gaps resulting from damage (cracks) or due to poor workmanship during the application of the fresh mortar [23]. Even if the application and curing conditions were optimal, a certain hydraulic resistance is expected due to the pore structure discontinuity between the materials [27].

The present paper aims to provide a comprehensive hygric description of several porous building materials traditionally used in masonry structures. First, the properties of single constituent materials –fired-clay brick, cement-based mortar and natural hydraulic lime (NHL) mortar– are studied. Subsequently, multi-layered masonry specimens made up of fired-clay bricks and lime mortar are analyzed. Thus, the existence of interfacial phenomena is assessed by comparing the behavior of each material separately and in combination with one another. The composite behavior of masonry elements is studied in terms of water absorption and isothermal drying tests. Finally, special focus is set on contrasting the hygric properties of NHL mortar cast in molds with the same mortar cured in masonry bed joints. The different curing conditions

for these two cases are usually neglected but it is proven that this assumption may lead to erroneous estimations.

2. MATERIALS AND METHODS

This section presents a brief description of the studied materials, namely fired-clay brick (B), Portland cement mortar (CM), NHL mortar –molded (LM) and from masonry bed joints (LMJ) –, and masonry composites. Subsequently, the configuration of the specimens used throughout the study is introduced. Finally, a detailed explanation of the different experimental procedures is given.

2.1. Materials

2.1.1 Extruded fired-clay bricks

The masonry units selected for this study were commercial fired-clay solid extruded bricks. The extrusion process, as well as the drying and subsequent baking (or 'firing') were fully automated. According to the specifications of the manufacturer, the bricks were baked in a flash oven at 850°C for 3 hours. It must be noted that in this type of process, the actual baking temperature depends on the position of the units inside the oven, which may result in a certain level of variability between bricks of the same batch. Uneven heating of the brick mass is usually perceived within single units as well, which becomes apparent in the color transition between the outer layer and the core (Figure 1). Clay particles become more sintered at higher baking temperatures, resulting in a lower porosity and a more intense red color of the brick [27].

(a) (b)

Figure 1. Cross-sections of fired-clay brick units: (a) transversal section through the middle plane; (b) longitudinal section through the middle plane.

2.1.2 Portland cement mortar

Portland CEM I – 42.5R, as classified by EN 197-1:2011 [36], was used as a reference for comparison with the lime-based mortar used in this study. The cement mortar was prepared with a binder-aggregate ratio 1:5 by volume and water-binder ratio 1:3 by weight. After casting, the mortar was kept in controlled curing

conditions, 20ºC and 90% RH, for 48 hours. Then, the specimens were demolded and immersed in water at 20ºC for more than a year.

2.1.3 Natural hydraulic lime mortar

The lime mixes analyzed in this study were prepared using a commercial pre-mixed NHL-based mortar, NHL 3.5 (REABILITA Cal Consolidação). The mortar was prepared as suggested by the producer by blending 1 kg of the dry powder provided by the manufacturer with 0.15 kg water. For molded specimens, the freshly cast mortar was kept for 48 hours in controlled curing conditions, 20ºC and 90% RH. Then, the specimens were demolded and maintained in laboratory conditions, 20ºC and 60% RH, for more than a year.

2.1.4 Masonry

Masonry samples (brick + mortar) were extracted from a wall using a diamond coring wet drilling machine. The wall was constructed using the same bricks and NHL-based mortar discussed above. The bricks were docked in water before placement to prevent undesired suction of water from the fresh mortar. The average thickness of the mortar joints was 12 mm. Right after the wall was built, it was covered with a polyethylene sheet for 48 hours to prevent water evaporation. After that, the cover was removed and the wall was kept in laboratory conditions, 20ºC and 60% RH, for more than a year before the cores were extracted.

2.2. Specimens

Fired-clay extruded bricks were used in different formats depending on the corresponding test setup. Initially, whole brick units with nominal size 200 mm × 100 mm × 50 mm were tested. Subsequently, the external surfaces of the units were removed by grinding. Thus, the outermost brick layer (thickness 5 mm) was removed, and the resulting prisms were cut into smaller pieces for further testing (Figure 2).

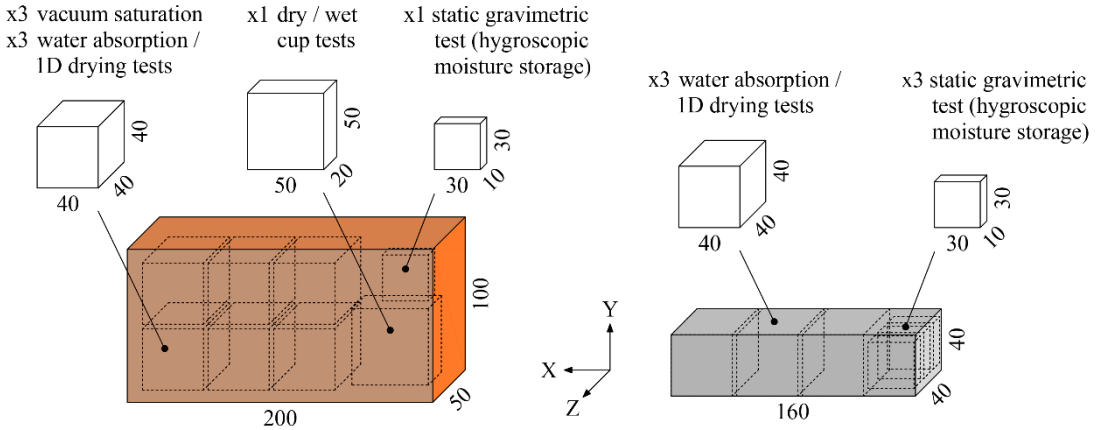

Figure 2. Cutting layout of brick units and mortar prisms (average dimensions in mm).

As for the mortars, standard molds with dimensions 160 mm × 40 mm × 40 mm were used to cast the different mixes. Initially, whole mortar prisms were used. Then, the prisms were cut into smaller pieces for further testing (Figure 2). Additionally, lime mortar discs extracted from masonry bed joints (Figure 3) were analyzed to determine differences with respect to the molded counterpart.

The multi-layered specimens extracted from the masonry wall consisted of cylinders with different stacking arrangements, i.e. different B+LMJ configurations (Figure 3). The average diameter of the cylinders was Ø=51.30 mm.

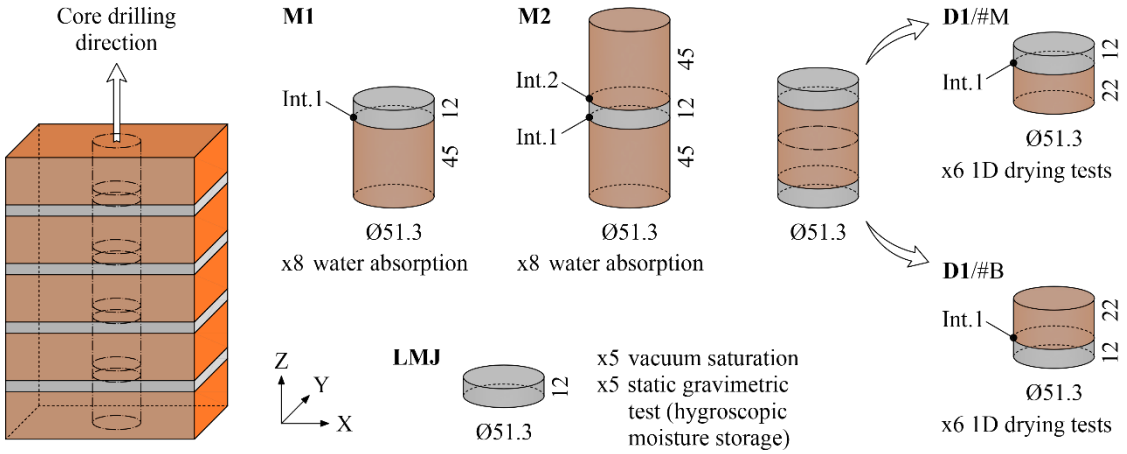

Figure 3. Lime mortar discs and multi-layered specimens extracted from masonry wall (schematic representation) (average dimensions in mm).

The number and type of specimens used for the characterization of single materials are summarized in Table 1. Likewise, the masonry specimens tested are summarized in Table 2.

Table 1. Number of single-material specimens tested.

Material	Specimen (dimensions in mm)	Test and test direction								
		Vacuum saturation	Sorption isotherm	Water absorption			1D drying test			Vapor permeability
				X	Y	Z	X	Y	Z	Z
B	200×100×50±2	10	--		5 (1)		--	--	--	--
	40×40×40±1	15 (2)	--	5 (3)	5 (3)	5 (3)	5 (4)	5 (4)	5 (4)	--
	50×50×20±1	--	--	--	--	--	--	--	--	5 (2)
	30×30×10±1	--	5 (2)	--	--	--	--	--	--	--
CM	160×40×40±0.5	4	--		4 (3)		--	--	--	--

	40×40×40±0.5	3 [5]	--	3 [3]	--	--	3 [4]	--	--	--
	30×30×10±1	--	3 [5]	--	--	--	--	--	--	--
LM	160×40×40±0.5	4	--	4 [3]			--	--	--	--
	40×40×40±0.5	3 [5]	--	3 [3]	--	--	3 [4]	--	--	--
	30×30×10±1	--	3 [5]	--	--	--	--	--	--	--
LMJ	Disc Ø51.3, h=12±1	5	5	--	--	--	--	--	--	--

[1] 5-brick unit subset chosen from the initial 10 brick units tested for vacuum saturation

[2] Cut from 5-brick unit subset

[3] Same specimens used for vacuum saturation

[4] Same specimens used for water absorption

[5] Cut from mortar prism

1

2 Table 2. Number of masonry specimens tested.

Masonry	Specimen (dimensions in mm)	Test and test configuration			
		Water absorption		1D drying test	
		+Z	-Z	Drying from brick	Drying from mortar
M1	Cylinder Ø51.3, h_B=45±1, h_{LMJ}=12±1	8	8 [1]	--	--
M2	Cylinder Ø51.3, h_B=45±1, h_{LMJ} =12±1	8	8 [1]	--	--
D1	Cylinder Ø51.3, h_B=22±2, h_{LMJ} =12±1	--	--	6	6

[1] Same specimens tested in the opposite direction

3

4 **2.3. Methods**

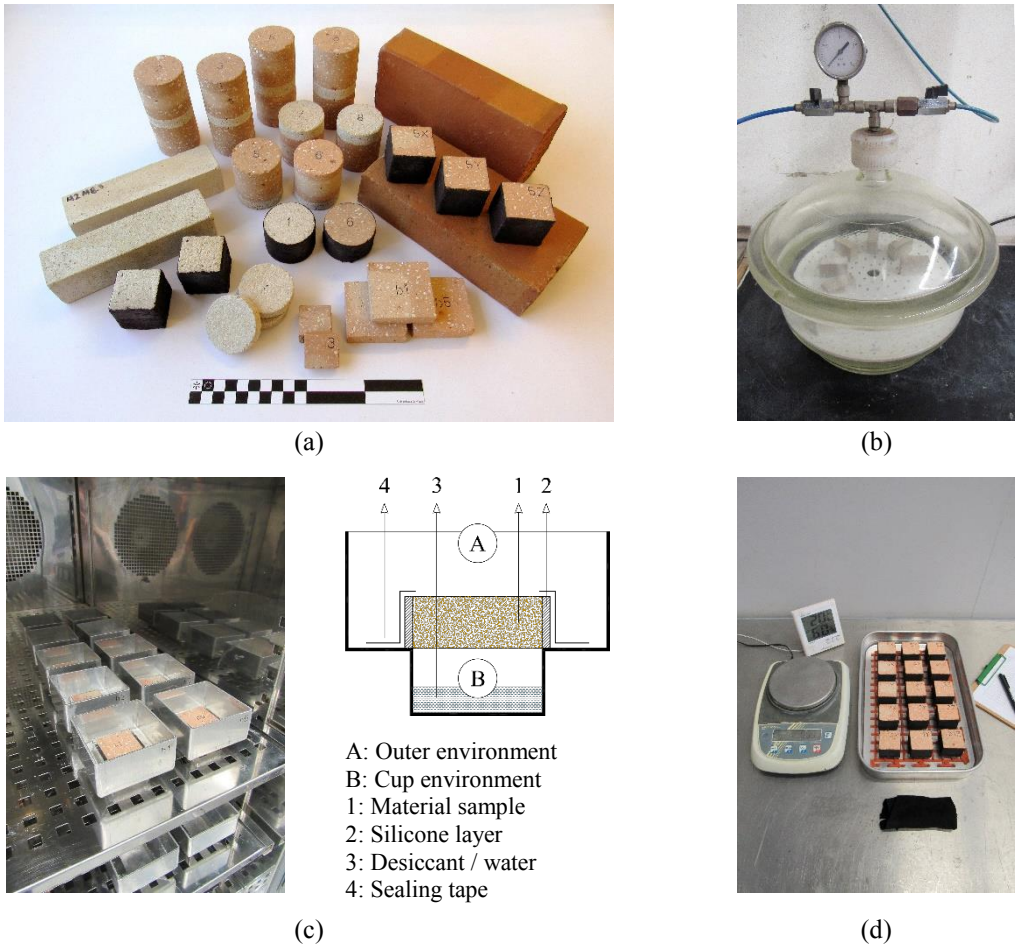

Figure 4. Examples of specimens and test setups used to determine hygric properties: (a) selection of material samples; (b) vacuum saturation; (c) cup test; (d)capillary absorption.

2.3.1 Oven-drying for pre-conditioning of samples

Most experimental methods applied in the current study required an initial pre-drying of the materials. Such initial pre-conditioning was performed by means of oven-drying in accordance with ISO 12570 [37]. Oven-drying at 105ºC was used for fired-clay bricks. Conversely, the drying temperature was reduced to 70ºC for mortar and masonry specimens to avoid microstructural damage or removal of chemically bound water from the cementitious matrix [38]. The drying process was concluded when the change of mass between two consecutive weight measurements with a difference of at least 24 hours was less than 0.1% of the total mass of the specimen.

2.3.2 Vacuum saturation tests

Vacuum saturation tests were performed following the recommendations of RILEM TC [39] to determine open porosity, ϕ_o [-], bulk density, ρ_b [kg/m^3], and saturation moisture content, w_{sat} [kg/m^3]. The studied samples comprised brick units, mortar prisms, brick and mortar cubes, and bed joint mortar discs (Table

1). Due to the high variability usually shown by fired-clay bricks, a sample of 10 randomly chosen units belonging to the same batch was analyzed initially. Then, a subset of 5 statistically comparable specimens was selected for further studies. For mortar specimens, a sample of 4 prisms for each mortar type and 5 bed joint mortar discs were used.

Initially, the specimens were oven-dried following the procedure previously explained. The samples were left to cool down and then placed in an evacuation vessel where the pressure was lowered below 100 mbar to remove the air from the open pores of the material. The vacuum pressure was maintained for 4 hours. Subsequently, tap water at 15-20°C was gradually introduced into the vessel until the water level was 1-2 cm above the specimens. The vacuum was maintained during the introduction of water and for the following 4 hours. Subsequently, the system was set back to atmospheric pressure and the specimens were left under water for 24 hours. Finally, the immersed mass, m_{im} [kg], was determined by weighing under water (hydrostatic weighing). Then, the specimens were wiped with a dampened cloth and weighed in air to determine the saturated mass, m_{sat} [kg].

The bulk volume, V_{bulk} [m^3], was calculated from the masses measured in air and under water as:

$$V_{bulk} = \frac{m_{sat} - m_{im}}{\rho_w} \quad (1)$$

where ρ_w [kg/m^3] is the density of water, assumed 1000 kg/m^3 in normal conditions. Consequently, the bulk density, ρ_{bulk} [kg/m^3], was calculated as:

$$\rho_{bulk} = \frac{m_{dry}}{V_{bulk}} \quad (2)$$

Similarly, the open porosity, ϕ_o [dimensionless], was calculated as:

$$\phi_o = \frac{m_{sat} - m_{dry}}{m_{sat} - m_{im}} \quad (3)$$

Saturation moisture content, w_{sat} [kg/m^3], was derived from open porosity as:

$$w_{sat} = \phi_o \cdot \rho_w \quad (4)$$

The total porosity, i.e. open + closed porosity, was not studied since the volume of closed pores does not take part in moisture transport.

2.3.3 Static gravimetric tests

The sorption isotherms (adsorption/desorption) of the materials were obtained through static gravimetric tests according to ISO 12571 [40]. The sorption isotherms represent the moisture storage capacity of a material in the hygroscopic range, namely from dry state, i.e. 0% RH, to 93-95% RH. In the over-hygroscopic or capillary range, i.e. above 93-95% RH, the sorption isotherms become extremely steep and slight variations in relative humidity result in large changes in moisture content. Thus, the higher part of the moisture storage curve must be completed by other means, namely pressure plate experiments or results derived from mercury porosimetry [41].

The size of the specimens used for these tests (Table 1) was chosen following the recommendations by Feng *et al*. [38], who proved that smaller specimens help speed up the process without compromising the accuracy. Brick and mortar specimens were cut from the brick units and mortar prisms used for the previous tests (Figure 2): 1 brick piece from each unit (5 replicates in total) and 3 mortar pieces from a single prism (3 replicates for each type of mortar). Additionally, lime mortar discs extracted from masonry bed joints (5 replicates) were tested as well.

To define the sorption isotherms, the equilibrium moisture content of the materials was determined at different relative humidity levels. It must be noted that the moisture content is usually expressed either as mass of adsorbed water per volume of dry material, w [kg/m^3], or as mass of adsorbed water per mass of dry material, w_g [kg/kg]. The latter format, known as gravimetric moisture content, is used for the static gravimetric tests. Nonetheless, both expressions are related through:

$$w = w_g \cdot \rho_{bulk} \tag{5}$$

Both adsorption and desorption were studied to assess the existence of hysteresis. The adsorption process started with initially dry samples and then, consecutive higher RH levels were imposed. A climatic chamber was used to provide constant RH levels and isothermal conditions (T=23±1ºC). For each level, the moisture content of the specimens was determined periodically. Equilibrium was considered when 3 successive weight measurements at intervals of at least 24h showed a relative mass variation below 0.1%. Once the equilibrium was attained, the environmental RH was set to a new level. After the last step of the adsorption process (95% RH), the samples were saturated by immersion in water at atmospheric pressure. The specimens were taking out of the bath periodically and weighed until the water mass gain had reached a plateau. The saturation state attained at the end of this process was considered analogous to the capillary moisture content obtained via capillary absorption tests, $w_{g,cap}$ [kg/kg]. Subsequently, the desorption

process began, following a sequence of decreasing RH levels. The discrete measurement points determined with this method were then used to fit the moisture storage function of the materials by means of analytical expressions.

2.3.4 Cup tests

Cup tests were performed on brick samples following the specifications of ASTM E96/E96M−10 [42], ISO 12572 [43], and EN 15803 [44], to determine the water vapor permeability, δ_v [kg/(m·s·Pa)], or alternatively the water vapor resistance factor, μ [dimensionless]. Both properties are related by:

$$\delta_v = \frac{\delta_a}{\mu} \tag{6}$$

where δ_a [kg/(m·s·Pa)] is the water vapour permeability in still air, defined empirically [44]:

$$\delta_a = 2.31 \cdot 10^{-5} \frac{P_0}{P \cdot R_v \cdot T} \left(\frac{T}{273.15}\right)^{1.81} \tag{7}$$

where $P_0 = 101325$ [Pa] is the standard atmospheric pressure, P [Pa] is the ambient barometric pressure, $R_v = 461.5$ [J/(kg·K)] is the universal gas constant for water vapour, and T [K] is the temperature.

These tests are based on stationary diffusion analysis in which the studied material acts as a filter between two environments with different vapor pressures. The test is defined as dry or wet cup depending on whether the relative humidity inside the cup is lower or higher than outside, respectively. The gradient of vapor pressure between the internal and external surfaces leads to a vapor flux across the specimen. By determining this vapor flux, the vapor permeability of the material can be derived:

$$\delta_v = \frac{g \cdot t}{\Delta P_v} = \frac{(G/A) \cdot t}{\Delta P_v} \tag{8}$$

where g [kg/(s·m^2)] is the rate of water vapor flow, G [kg/s] is the average mass change rate, A [m^2] and t [m] are the exposed area and the thickness of the test specimen, respectively, and ΔP_v [Pa] is the vapour pressure difference between the two environments. The vapor pressure is calculated from the definition of relative humidity, φ [dimensionless]:

$$\varphi = \frac{P_v}{P_{v,sat}(T)} \tag{9}$$

where the saturation vapor pressure, $P_{v,sat}$ [Pa], is a non-linear function of temperature, T [K], and is described empirically by different authors, such as [45]:

$$P_{v,sat} = 610.7[\text{Pa}] \cdot 10^{7.5\left(\frac{T-273.15}{T-35.85}\right)} \quad (10)$$

In the present work, the cups were customized to the shape and dimensions of the specimens (Figure 4), which were cut out from the previously studied units (Figure 2). One specimen per brick was studied, thus a total of 5 tested replicates. A thin layer of neutral silicone was applied to the lateral faces of the specimens to guarantee one-dimensional transport. The conditions used for the cup tests in this study are summarized in Table 3. The tests were performed inside a climatic chamber to ensure constant environmental conditions, namely 23°C and 55% RH. The specimens were pre-conditioned in the same environment until equilibrium was reached. Then, the cups were prepared by placing a piece of cotton saturated with distilled water (wet procedure) or silica gel desiccant (dry procedure) on the bottom of the container. The specimens were then placed and sealed on the opening of the cup with adhesive aluminum tape to guarantee a vapor-tight system. The time was recorded from the moment when the system was sealed, and the evolution of mass was registered periodically. The tests were concluded when a clear linear trend ($R^2 > 0.99$) could be established using at least 5 successive points measured at intervals of not less than 24 hours.

Table 3. Environmental conditions for cup tests.

Method	ϑ_{env} [°C]	RH_{env} [%]	RH_{cup} [%]	ΔP_v [Pa]
Dry cup	23	55	3	1460.6
Wet cup	23	55	98	1207.8

For the processing of results, the masked edge effect was considered negligible. Conversely, the air layer resistance inside the cup was taken into account according to ASTM E96/E96M−10 [42] and ISO 12572 [43]. Additionally, the air velocity above the specimens was assumed to be below 1 m/s. Thus, an exterior surface transfer resistance was considered as well, and the corresponding correction was introduced according to ASTM E96/E96M−10 [42].

2.3.5 Capillary absorption tests

Capillary absorption tests were performed according to the specifications of EN ISO 15148 [46] to determine the capillary absorption coefficient, A_w [kg/m^2/s$^{0.5}$], and capillary moisture content, w_{cap} [kg/m^3]. The tests were performed on whole brick units, brick cubes, mortar prisms, mortar cubes, and masonry cylinders (Table 1, Table 2). The bricks used for the vacuum saturation tests were used here again,

i.e. 5 statistically comparable brick units. The same specimens were tested in all three directions (X, Y, Z). Once the whole units were tested, brick cubes were cut out (Figure 2) for further water absorption tests. Thus, 3 cubes (1 for each testing direction) were extracted from each brick, resulting in 3 groups of 5 replicates for each direction. For the mortars, the specimens consisted of the same specimens used for vacuum saturation tests, i.e. 4 molded prisms for each mortar type. The same specimens were studied in all three directions (X, Y, Z). Moreover, mortar cubes were cut out from a mortar prism of each type (Figure 2). Therefore, 3 mortar cubes were analyzed as well (testing direction X). Finally, water absorption tests were performed on masonry cylinders with different B+LMJ configurations, in the direction perpendicular to the joints.

Before the tests, the specimens were oven-dried according to the procedure previously introduced. After cooling down, the lateral faces of the specimens were wrapped with adhesive aluminum tape to prevent evaporation and guarantee a 1-D moisture flow. Nevertheless, the bottom part of the lateral faces (8-10 mm) was left unwrapped to avoid interfacial water uptake between the brick surface and the film. Additionally, the uppermost face was left uncovered to facilitate air evacuation. The specimens prepared in this way were then placed into a shallow water basin so that they were submerged 5 mm approximately. The level of the water was kept constant throughout the test. Note that the water used during the test was conditioned to room temperature beforehand to avoid temperature-dependent phenomena associated with the change of viscosity of the water [47]. The tests were performed in a climatic chamber with controlled laboratory conditions, namely 20ºC and 60% RH. The specimens were regularly taken out of the bath, the excess water was removed with a dampened cloth, and the weight was measured. The water absorption coefficient was then determined by the one-tangent method: the water mass inflow per unit area was plotted against the square root of time and the slope of the initial linear trend (first stage) was defined as A_w. The tests terminated when the inflow reached a plateau (second stage). The average value of the last three points in the plateau was defined as the capillary moisture content, w_{cap}.

When the same specimens were planned to be studied in different directions, i.e. brick units and mortar prisms, after the conclusion of each test, the specimens were unwrapped and oven-dried before the subsequent analysis in a different direction. For the specimens that were tested just once, i.e. brick and mortar cubes, a neutral silicone was chosen to cover the lateral faces. For these cases, the full height of the lateral faces was covered assuming that no water uptake would occur between the interface of the two materials, i.e. silicone and substrate.

For the case of masonry cylinders, a transparent adhesive film was used to wrap the lateral surfaces. Different configurations of masonry composites were studied (Figure 3). The first set was made up of 8 cylinders with 2 layers (1 interface), i.e. B+LMJ. The specimens were tested twice, once sucking up water from the mortar side and the second time absorbing water from the brick. The second group of masonry specimens was composed of 8 cylinders with 3 layers (2 interfaces), namely B+LMJ+B. Similarly, these cylinders were tested twice, each time sucking up the water from a different brick. The purpose of these tests was to verify the existence of a hydraulic resistance at the interface between the two materials.

2.3.6 Drying tests

Isothermal, one-dimensional drying tests were carried out following the recommendations of EN 16322 [48], i.e. subjecting initially capillary saturated specimens to 1-D drying from a single surface. These tests were used to study the drying kinetics of the selected materials. Furthermore, drying results may be used for the identification of transport properties, such as liquid permeability, by means of inverse modelling [49].

The tests were performed on a total of 15 brick cubes (5 specimens for each direction, i.e. X, Y, Z) and 3 mortar cubes for each mortar type (testing direction X) which were initially saturated by means of capillary absorption tests. Once the capillary moisture content was attained, w_{cap}, the specimens were kept partially immersed in water and the upper face was sealed using neutral silicone (note that the lateral faces were already sealed with the same material prior to capillary tests). Once the silicone was dry, the specimens were placed in a climatic chamber with controlled environmental conditions, namely 23ºC and 55% RH, to dry from the unsealed surface. The specimens were weighed periodically to establish the mass loss until a plateau was reached.

Drying tests were also performed on masonry cylinders (Figure 3). The initial cylinders were made up of three layers, namely LMJ+B+LMJ. Subsequently, they were cut in half, so two pieces LMJ+B were obtained. The pieces were then prepared following the same procedure described for the single-material cubes. From each pair, one was prepared to dry from the mortar face and the other one to dry from the brick. A total of 12 specimens were tested, 6 per case.

3. RESULTS AND DISCUSSION

3.1. Results on single constituent materials

3.1.1 Vacuum saturation tests results

The properties derived from vacuum saturation tests are collected in Table 4.

Table 4. Results from vacuum saturation tests (CoV between parentheses).

Material	ρ_{bulk} [kg/m^3]	ϕ_o [-]	w_{sat} [kg/m^3]
B	1900	0.280	280
	(2.69)	(6.76)	(6.76)
CM	2000	0.210	210
	(0.15)	(1.05)	(1.05)
LM	1990	0.255	255
	(0.81)	(2.53)	(2.53)
LMJ	2060	0.230	230
	(1.32)	(6.93)	(6.93)

Vacuum saturation tests performed on whole bricks and brick cubes extracted from those initial units produced the same results in terms of bulk density and open porosity. Similarly, no difference was observed between mortar prisms and mortar cubes cut out of them. Therefore, the use of smaller specimens is justified and is indeed recommended to speed up the process and guarantee the saturation of the innermost spaces.

As it was expected, the properties of the lime mortar obtained from masonry bed joints differed from those obtained from molded specimens even though the mixes were prepared with the same composition and in the same controlled environment. Overall, LMJ showed higher bulk density and lower open porosity, and consequently lower saturation moisture content.

3.1.2 Moisture isotherm

The data collected from static gravimetric tests are shown in Figure 5. The results showed clear similarities between B and LM, whereas CM and LMJ followed a different trend. On one hand, B and LM hardly showed moisture adsorption until high RH values, revealing a low hygroscopic response. Moreover, no significant differences were found between adsorption and desorption. Conversely, hysteresis was observed in CM and LMJ. CM showed considerable moisture adsorption for lower RH levels, confirming a markedly hygroscopic nature. Likewise, LMJ showed moisture adsorption for lower RH levels, and therefore a more hygroscopic response than its molded counterpart.

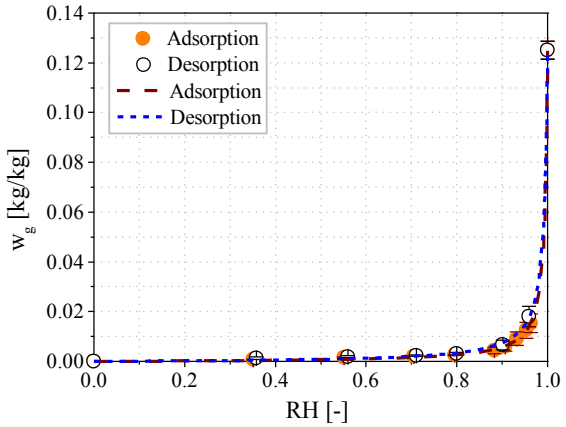
Adsorption
Desorption
Adsorption
Desorption
w_g [kg/kg]
RH [-]
0.00
0.02
0.04
0.06
0.08
0.10
0.12
0.14
0.0
0.2
0.4
0.6
0.8
1.0

(a)

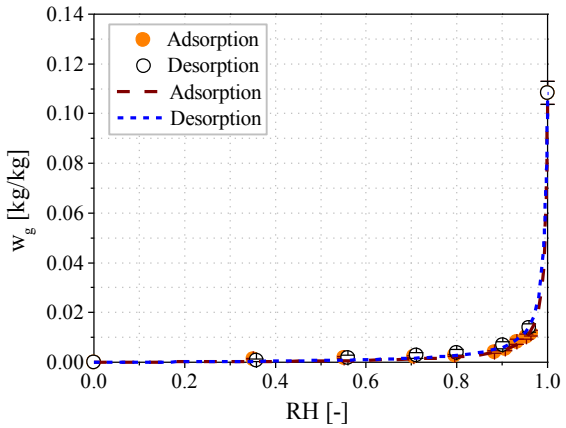
Adsorption
Desorption
Adsorption
Desorption
w_g [kg/kg]
RH [-]
0.00
0.02
0.04
0.06
0.08
0.10
0.12
0.14
0.0
0.2
0.4
0.6
0.8
1.0

(b)

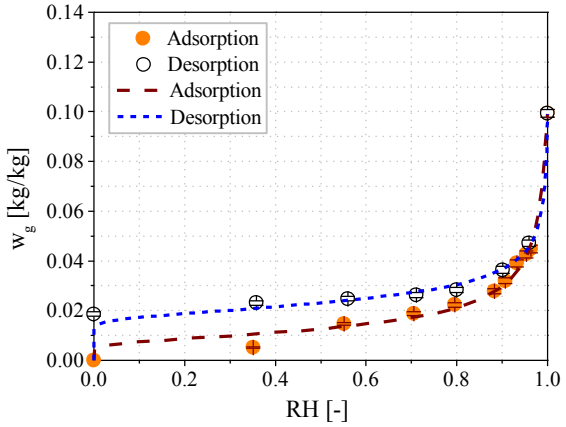
Adsorption
Desorption
Adsorption
Desorption
w_g [kg/kg]
RH [-]
0.00
0.02
0.04
0.06
0.08
0.10
0.12
0.14
0.0
0.2
0.4
0.6
0.8
1.0

(c)

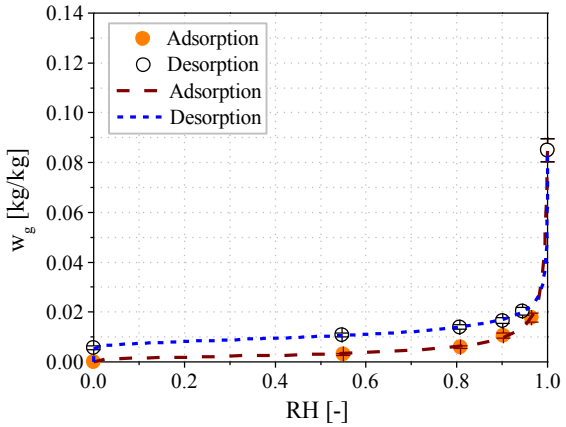

(d)

Figure 5. Sorption isotherms and fitting curves for the studied materials at 23°C: (a) B, and (b) LM, fitted with Künzel's model [50]; (c) CM, and (d) LMJ, fitted with Mualem's model [51].

The experimental measurements were fitted with common analytic expressions found in the literature. In particular, the model proposed by Künzel [50] was used to describe the sorption behavior of B and LM. For CM and LMJ, the model established by Mualem [51] was adopted. The expression proposed by Künzel can be written as [50]:

$$w(\varphi) = w_{cap} \cdot \frac{(\psi - 1) \cdot \varphi}{\psi - \varphi} \tag{11}$$

where $w(\varphi)$ [kg/m^3] is the moisture content as a function of relative humidity, φ [dimensionless], w_{cap} [kg/m^3] is the capillary moisture content, and ψ [dimensionless] is a fitting parameter. Künzel's model stems from a simplified form of the BET equation [52] and applies to sorption curves with a marked exponential trend, i.e. non-hygroscopic, capillary-active materials.

On the other hand, the model proposed by Mualem [51] is extensible to hygroscopic materials. This model is a constrained form of the more generalized equation proposed by van Genuchten [53]:

$$w(P_c) = w_{cap} \cdot [1 + (a \cdot P_c)^n]^{-m} \tag{12}$$

where $w(P_c)$ [kg/m^3] is the moisture content as a function of capillary pressure, P_c [Pa], and a [1/Pa], n [dimensionless] and m [dimensionless] are fitting parameters. Capillary pressure and relative humidity are related by $P_c = \rho_w \cdot R_v \cdot T \cdot \ln \varphi$, known as Kelvin equation. Considering van Genuchten's expression, Mualem fixed $m = 1 - 1/n$ [51]:

$$w(P_c) = w_{cap} \cdot \left[1 + (a \cdot P_c)^{1/(1-m)}\right]^{-m} \quad (13)$$

The curves obtained from these analytic expressions are plotted in Figure 5 together with the experimental points. The corresponding fitting parameters for the different cases are presented in Table 5 together with relevant criteria to evaluate the accuracy of the model. In this case, the accuracy was determined by the adjusted coefficient of determination (R^2_{adj}) and the normalized root mean square error (%NRMSE) between predicted and measured points. The adjusted R^2 takes into account the effect of the number of fitting parameters and is given as:

$$R^2_{adj} = \frac{(N-1)R^2 - (M-1)}{N-M} \quad (14)$$

where N is the number of measured data and M is the number of fitting parameters.

The %NRMSE is expressed as a percentage and is defined as follows:

$$\%NRMSE = \frac{1}{\sum_{i=1}^{N} x_{exp,i}/N} \sqrt{\frac{1}{N}\sum_{i=1}^{N}\left(x_{exp,i} - x_{pre,i}\right)^2} \quad (15)$$

where x_{exp} and x_{pre} are the measured values from the experiments and the predicted values from the fitted curves, respectively. A lower value of %NRMSE indicates a better match.

Table 5. Fitting parameters and accuracy of the modelled sorption isotherms.

Material	Künzel (Eq. (11))	Mualem (Eq. (13))	R^2_{adj}	%NRMSE
B	$\psi_{ads} = 1.0055$	--	0.999	2.30%
	$\psi_{des} = 1.0070$	--	0.999	2.49%
LM	$\psi_{ads} = 1.0052$	--	0.999	5.30%
	$\psi_{des} = 1.0066$	--	0.999	4.49%
CM	--	$a_{ads} = 9.40 \cdot 10^{-7}$ [1/Pa] $m_{ads} = 0.312$	0.993	6.62%
	--	$a_{des} = 4.00 \cdot 10^{-6}$ [1/Pa] $m_{des} = 0.197$	0.983	7.77%
LMJ	--	$a_{ads} = 2.76 \cdot 10^{-6}$ [1/Pa] $m_{ads} = 0.325$	0.996	7.94%
	--	$a_{des} = 2.00 \cdot 10^{-6}$ [1/Pa] $m_{des} = 0.326$	0.994	7.96%

3.1.3 Vapor permeability

The results from dry and wet cup tests performed on brick specimens gave $\mu_{dry} = 34.14$ (CoV = 12.64%) and $\mu_{wet} = 13.50$ (CoV = 17.85%), respectively. Vapor permeability was only tested in the bed direction (Z) since the cutting of the original units after removal of the outermost layer (5 mm) did not allow to obtain the specimens for the other directions (Figure 2). It must be noted that the results obtained from cup measurements showed the highest scatter among the tests performed in this study. Low reliability for this type of test has been indicated before, see e.g. [16–18,54].

The water vapor resistance factor, μ, indicates how many times lower the vapor diffusion in the material is in comparison with vapor diffusion in still air. By definition, $\mu = 1$ for stagnant air. Expressing the water vapor permeability through the vapor resistance factor by means of Equation (6) has the advantage of assigning the temperature and pressure dependencies of water vapor diffusion to the empirical term $\delta_a(T, P)$, so that the vapour resistance factor is independent of these variables and becomes a constant characteristic for each material. Nonetheless, as the values for our brick specimens show, vapor diffusion tests performed at different relative humidity levels, e.g. dry and wet cups, usually result in different permeability values for the same material [12,13]. Consequently, vapor diffusion (expressed through either vapor permeability or vapor resistance factor) must be a function of moisture content. There have been considerable efforts in the literature to explain this phenomenon, e.g. [11,41,50], but a univocal standpoint has not been reached. Most authors agree on the overall influence of the pore-saturation level since the presence of water islets in the pore system modifies the effective space available for vapor diffusion [11]. However, the debate appears when defining the effect of moisture condensation in the pores for high moisture contents and subsequent reduction of the space accessible to vapor transport. Künzel [50] argued that vapor diffusion might be either obstructed or –this is the most common assumption– enhanced through the water islets depending on the local conditions of temperature and moisture content inside the material. Conversely, Krus [41] introduced the phenomenon of surface diffusion, i.e. advective water transport along the adsorbed liquid film on pore walls, to explain the differences observed experimentally between dry and wet cup tests. Surface diffusion becomes noticeable at high humidity levels, but in practice, it cannot be distinguished from vapor transport and therefore it is lumped together with diffusion, which could cause the observed differences in apparent vapor permeability. The additional liquid transport superimposed on diffusion would be likely to increase the observed vapor permeability, therefore providing a lower

resistance value for wet cup measurements. Indeed, this is in agreement with the observations made for the brick specimens in our study.

3.1.4 Capillary absorption

Water uptake tests for material characterization were performed on whole units, brick cubes and mortar prisms in different directions. The results are summarized in Table 6.

Table 6. Results from water absorption tests (CoV between parentheses).

Material	$A_{w,\mathrm{X}}$ [kg/m^2/s$^{0.5}$]	$A_{w,\mathrm{Y}}$ [kg/m^2/s$^{0.5}$]	$A_{w,\mathrm{Z}}$ [kg/m^2/s$^{0.5}$]	A_w (1) (2) [kg/m^2/s$^{0.5}$]	w_{cap} (2) [kg/m^3]
B units	0.118	0.090	0.068	--	250
	(8.43)	(5.51)	(7.36)		(2.35)
B cubes	0.104	0.089	0.061	--	240
	(6.31)	(7.78)	(5.86)		(1.07)
LM (3)	0.237	0.234	0.233	0.235	225
	(1.62)	(1.59)	(1.46)	(1.57)	(2.05)
CM (3)	0.059	0.059	0.060	0.059	180
	(3.96)	(5.32)	(7.77)	(6.49)	(2.45)

(1) Isotropic

(2) Average of all tests

(3) Sample of 4 molded prisms

The capillary moisture content, w_{cap} [kg/m^3], was determined as the average moisture content at the end of the water absorption tests. It must be noted that in the literature, it is possible to find w_{cap} calculated as the moisture content at the intersection between linear approximations of the first and second stages of the capillary absorption test. However, for porous materials with a sharp transition between the two stages and a well-developed plateau during the second stage –such as the ones presented in this study–, w_{cap} calculated in one or the other way is equivalent. The capillary moisture content is always lower than the saturation moisture content defined from open porosity, i.e. $w_{cap} < w_{sat}$, due to air entrapment in the pore structure during imbibition [55]. For prolonged imbibition or immersion times, w_{cap} will approach w_{sat} as the air trapped in the pores dissolves into the water [11]. Therefore, w_{cap} is more a fuzzy limit than a fixed value. For the studied materials, the comparison between saturation and capillary moisture contents gave $w_{cap} \approx 80\% - 90\%\ w_{sat}$, which is an indication of the quantity of pores that can be classified as capillaries with

respect to the overall open porosity.

The results obtained for whole bricks are shown in Figure 6 for the three studied directions: a) header or extrusion direction, labelled X; b) stretcher direction, labelled Y; c) bed direction, labelled Z. Note that each set of tests ended up in a different plateau since the exposed surface was not the same for each case; nonetheless, the moisture content at the end of all tests was equivalent. The rate of absorption per unit area was fastest in the extrusion direction (X) and slowest in the bed direction (Z). Considering the bed direction as a reference –it is usually the most reported one–, we obtained $A_{w,B-X} \cong 170\%\, A_{w,B-Z}$ and $A_{w,B-Y} \cong 130\%\, A_{w,B-Z}$. This entails that the absorption behavior of a brick wall might be considerably underestimated if the properties of the bed face are generalized to other directions, e.g. lateral wetting from wind-driven rain. Note that the different cases analyzed here made use of the same specimens and the geometrical parameters do not influence the absorption process –water inflow normalized by area and heights too small to produce any significant pressure head–. Thus, the different behavior in the three directions can only be explained by an anisotropic pore system or by the existence of imperfections, such as hollows, fissures or cracks within the brick mass.

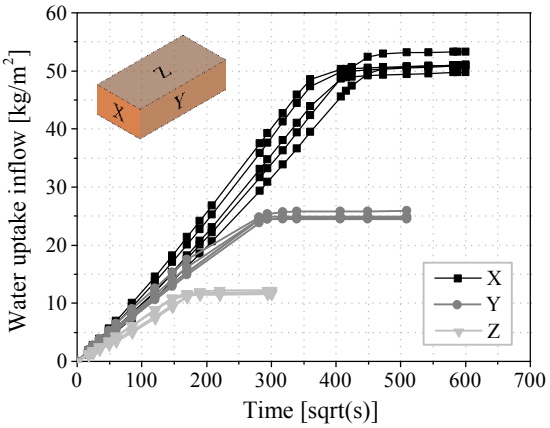

Figure 6. Water absorption results for brick units in the 3 studied directions.

The results of the water uptake tests in brick cubes are shown in Figure 7 for the three studied directions. The same overall trends observed in full-size bricks hold for the case of brick cubes: the capillary absorption rate was faster in the extrusion direction (X), followed by the stretcher direction (Y), and finally, bed direction (Z) was the slowest. Using the bed direction as a reference, $A_{w,b-X} \cong 170\%\, A_{w,b-Z}$ and $A_{w,Y} \cong 150\%\, A_{w,b-Z}$. In this occasion, the exposed area and height were equal for all specimens, so any geometrical influence was discarded. Consequently, the results point at an anisotropic structure of the

material, the presence of internal imperfections, or a combination of both.

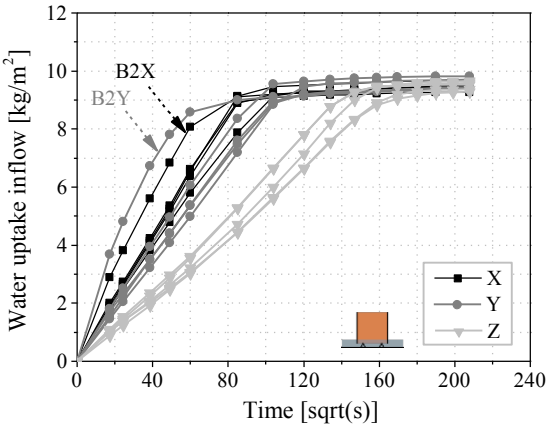

Figure 7. Water absorption results for brick cubes in the 3 studied directions.

By careful examination of the specimens, the main cause for the anisotropic behavior was associated with the existence of rifts or canals within the bulk mass of the brick. The reader is referred to Figure 1 where these imperfections are visible, with a more noticeable presence in the longitudinal direction. Therefore, the forming process of the bricks –in this case, extrusion– is deemed to be the reason behind the anisotropic behavior for water absorption. Furthermore, the impact of internal canals on the water uptake process may be observed in brick cubes B2X and B2Y (individuated in Figure 7). For these two cases, signs of absorbed water were spotted on the upper part of the specimens very early on in the process, starting from a particular location and spreading from there to the rest of the surface. This could be linked to the presence of a discontinuity across the specimen (bottom-to-top) from where the water was sucked up faster. In fact, the absorption curves for B2X and B2Y show a distinct non-linear trend with a faster absorption rate in comparison with the rest of the cases. Such behavior can be explained by the so-called "free-water" transport through canals (pores with diameter greater than 100 μm), which is faster than water suction through capillaries [56–58].

Overall, the results obtained from full-size bricks and brick cubes are comparable, as expected. However, the capillary moisture content and the water absorption coefficients (all 3 directions) are slightly higher for the whole bricks. As no size effect is expected in the capillary test results [59], these differences can be attributed to variations in the microstructure of the superficial layer of the bricks (which was removed in the cubes) compared to the core mass [18]. The existence of an external layer may be associated with the different temperatures reached during firing and consequently, different degrees of sintering of the clay and density/porosity values. Moreover, local defects associated with the manufacturing process, as mentioned

before, can be another reason for the observed difference in the capillary absorption coefficients obtained from brick units and brick cubes. Note that the brick cubes that showed evidence of canals were discarded for the calculation of average values although their curves are shown in the figures.

The results of the water absorption tests for CM and LM are shown in Figure 8. In contrast to the bricks, the results did not show significant deviations for different directions, confirming the isotropic behavior of these materials. The two mortars showed a noticeably distinct behavior: the absorption process in LM was the fastest, even faster than the bricks, whereas CM showed a very slow water uptake rate. Taking as a reference the water absorption coefficient for the bed direction of whole bricks, $A_{w,LM} \cong 335\%\ A_{w,B-Z}$ and $A_{w,CM} \cong 85\%\ A_{w,B-Z}$. Provided that these properties were directly applicable to multi-layered masonry walls, the expected absorption performance would vary considerably depending on the brick-mortar configuration. For combinations B+LM, the fastest path would be the mortar joint, whereas the joints in B+CM cases would act as a retardant barrier.

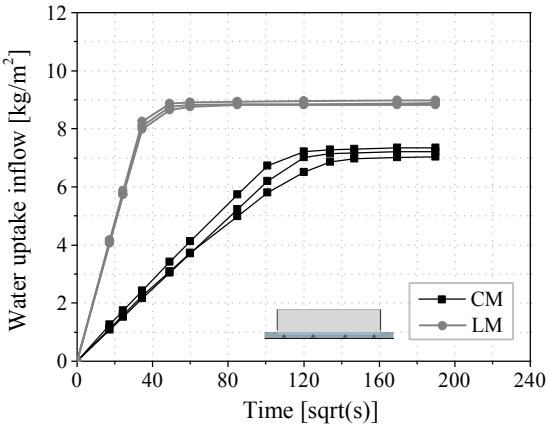

Figure 8. Water absorption results for cement mortar (CM) and lime mortar (LM) prisms.

Due to the small thickness of the specimens, the absorption tests on LMJ did not render reliable results in terms of water absorption coefficient. However, a clear plateau was reached at the end of the tests, from where capillary moisture content was calculated, $w_{cap,LM-joint} = 185$ kg/m^3 (CoV = 6.47%). This value is in agreement with the relation $w_{cap} \approx 80\% - 90\%\ w_{sat}$, observed for the other materials.

Comparison of water absorption rates between different materials has to be done with caution. It must be borne in mind that the water absorption coefficient is a phenomenological parameter and does not describe any real physical property. After all, different pore systems may result in the same water absorption coefficient, e.g. a small group of coarse pores may produce the same water absorption rate as a greater

amount of small pores [31].

3.1.5 Drying

The mass loss curves obtained from isothermal 1-D drying tests in brick cubes are shown in Figure 9 for the three studied directions. The results are expressed in terms of gravimetric moisture content. Considering the rate of mass loss, three main stages may be distinguished in the global drying process of porous materials. During the initial phase or Stage I, there is a high concentration of moisture at the surface of the material and the drying rate is controlled by environmental conditions, such as wind speed, air temperature, air humidity, etc. [30]. At this stage, the drying rate is constant, which is evidenced by a linear mass loss. In this phase, moisture transport within the material is faster than the mass transfer to the atmosphere at the surface. Stage II begins when the moisture supply to the surface can no longer balance the evaporation rate. In other words, the amount of water moved to the surface by capillary transport is less than the liquid being evaporated. Accordingly, the drying rate drops, and the drying process becomes dependent on the moisture transport properties of the material. The last phase or Stage III is characterized by a residual, slow drying rate, close to steady-state condition. The beginning of this phase is not clear-cut and is usually established as a virtual limit [60]. At this stage, the liquid water movement is limited to the thinnest pores that remain saturated or partially saturated in equilibrium with the environment and the main mechanism of moisture transport is vapor diffusion [61].

The drying curves of brick cubes (Figure 9) evidence the first and second stages while the third phase is not present. The first stage is identical for all the directions whereas slight differences appear in the second one. Since the second phase is dependent on the transport properties of the bricks, the differences between the samples can be attributed to the anisotropic behavior previously shown. Indeed, drying trends are consistent with the capillary water absorption results: faster drying is observed in the extrusion direction (X), followed closely by the specimens oriented in the stretcher direction (Y), and finally bed direction (Z) specimens reached equilibrium more slowly.

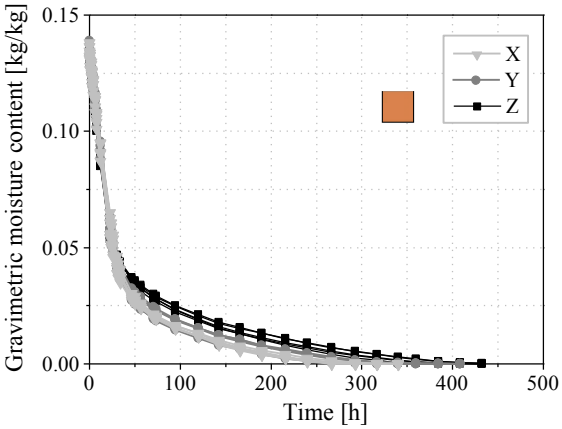

Figure 9. Drying test results for brick cubes in the 3 studied directions.

The mass loss curves obtained from drying tests in mortar cubes are shown in Figure 10 for the two types of mortar studied. Mortar specimens were tested only in one direction (longitudinal with respect to the original molded prism, X) since the isotropic hygric behavior was confirmed by the previous analyses. It is noticeable that the drying of CM is much slower than B or LM. Moreover, the steady-state condition reached at the end of the test reveals the hygroscopic nature of CM, i.e. the material still withholds a certain amount of water when equilibrium at 55% RH is reached through desorption from capillary saturation. This is in agreement with the observed moisture storage behavior (Figure 5c).

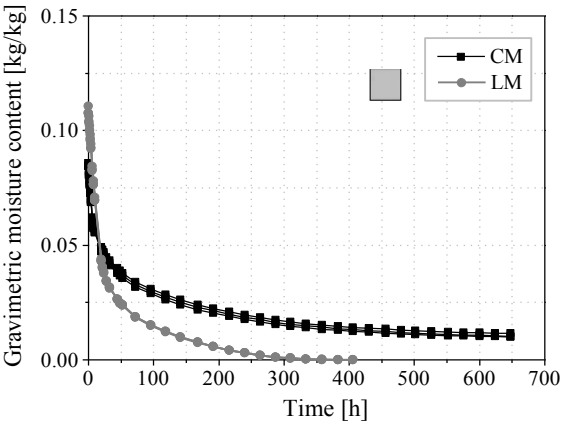

Figure 10. Drying test results (X direction) for cement mortar (CM) and lime mortar (LM) cubes.

The drying process is highly dependent on the boundary conditions. Higher temperature or lower air humidity would result in enhanced mass transfer and therefore higher drying rates (steeper mass loss). The fact that the first drying phase is not dependent on the material is demonstrated in Figure 9 and Figure 10, where the initial slope of the mass loss curves is the same for all the studied cases. Considering equivalent environmental conditions, the duration of the first drying stage depends on the material capacity to transport

liquid water towards the surface where evaporation occurs. Therefore, it provides information about how easily liquid water flows through the medium. In the case of the bricks, the range of constant drying rate extends from the initial capillary moisture content, w_{cap}, until 30-40% w_{cap}, in line with the studies by Hall and Hoff [62]. LM follows a similar trend, with the first drying stage ending at a moisture content value of about 40% w_{cap}. Finally, CM shows a very short first phase that finishes at approximately 70% w_{cap}. The development of the second drying stage is also indicative of the liquid water permeability of the material. Thus, a shorter second phase is registered for strongly capillary-active materials, e.g. B and LM. Conversely, a long, gradual second stage is generally observed in materials with a more pronounced hygroscopic behavior, such as CM.

Given the relationship between the drying rate during Stage I and the environmental conditions, the mass loss during the initial phase may be used to determine the convective flux transfer coefficient by means of inverse calculation. The mass transfer coefficient can be calculated from the first drying phase assuming constant vapor flux and constant boundary conditions [11]:

$$\beta = \frac{j_v}{P_v\left(T_{surf}, \varphi_{surf}\right) - P_v(T_{env}, \varphi_{env})} \tag{16}$$

where j_v [kg/(m^2·s)] is the vapor mass flow density, and P_v [Pa] is the vapour pressure calculated from Eq. (9)–(10). The relative humidity at the material surface can be assumed 100% during the first drying phase. This leads to a mass transfer coefficient $\beta = 6.50 \cdot 10^{-8}$ [s/m].

3.2. Results on masonry composites

3.2.1 Capillary absorption tests

The results of the capillary absorption tests for two-layer (1 interface) masonry composites are shown in Figure 11 for the two studied directions, namely B-to-LMJ, labelled M1-B (Figure 11a), and LMJ-to-B, labelled M1-M (Figure 11b). The cross-sectional area of all the cylinders is the same so a direct comparison of the water uptake mass is possible. Note that the tests for the configuration M1-M were concluded before the brick reached capillary saturation.

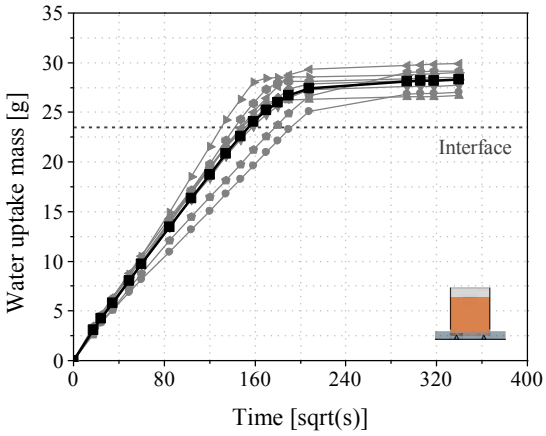

(a)

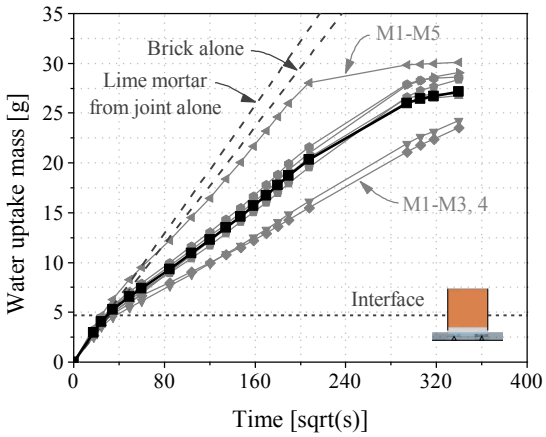

(b)

Figure 11. Water absorption results for masonry specimens M1 (B+LMJ): (a) B-to-LMJ configuration, M1-B; (b) LMJ-to-B configuration, M1-M. Grey curves represent test results and the black curve is the average. The location of the interface is estimated from the average volume of each material layer.

By comparison of the two cases in Figure 11, it is evidenced that the uptake rate is influenced by the presence of the interface. In Figure 11b, the slope of the moisture inflow per square root of time falls after a point. This point is identified as the interface and matches the expected capillary saturation for LMJ calculated as the average $w_{cap,LMJ} \cdot V_{bulk,LMJ} \cong 4.60$ g. Above the interface, the uptake mass curves are less steep than expected from the absorption rate of B alone. Similarly, the location of the interface in Figure 11a is estimated from the capillary saturation of the brick layer calculated as the average $w_{cap,B} \cdot V_{bulk,B} \cong 23.50$ g. However, the influence of the interface for the M1-B cases is less evident. This may be explained by several reasons, namely the smaller thickness of the mortar layer, which causes any difference to dissipate faster; and the higher suction capacity of the mortar, which counteracts the apparent retardant

effect of the interface. Moreover, the further the distance of the interface with respect to the water source, the lower the interfacial effect [63].

Dissimilar properties have been already discussed between LM and LMJ (Table 4). These differences were also evidenced in the water uptake tests for composite cylinders. Considering the first portion of the uptake curves in Figure 11b, the average water absorption coefficient for LMJ is $A_{w,LMJ} = 0.076$ [kg/m^2/s$^{0.5}$] (CoV: 7.39%), which is about three times smaller than the coefficient obtained for LM (Table 6). In turn, the average water absorption of the brick counterparts (initial slope of the curves in Figure 11a), $A_{w,B} = 0.073$ [kg/m^2/s$^{0.5}$] (CoV: 11.25%), was slightly higher than the value obtained for brick units in the same direction (bed or Z), though still in the same range (Table 6). Thus, the water absorption coefficient of LMJ turned out to be similar to that of the adjacent B.

From the results for M1-M (Figure 11b), it is possible to distinguish a global trend with upper (M1-M5) and lower (M1-M3, M1-M4) boundaries. To a greater or lesser extent, all cases revealed an absorption rate reduction associated with the presence of the interface. In general, two main factors may explain the absorption rate drop: a) the nature and quality of the interface, namely the presence of cracks, voids, or discontinuities; and b) the hydraulic affinity of the materials in contact, which has to do with the pore structure of each material. For instance, assuming cylindrical pores, the Young-Laplace equation defines the pressure at which a pore fills (or empties) according to its pore opening size:

$$p_c = \frac{2\sigma}{r} \cdot \cos(\gamma) \tag{17}$$

where σ [N/m] is the surface tension, r [m] is the pore radius, and γ is the contact angle. According to Eq. (17), a material with finer pores will exert higher capillary pressure and thus withhold water when in contact with a material with bigger pores. Furthermore, even if the material can withdraw the water from the previous layer, its absorption rate will be limited by the behavior of the source material. This phenomenon was defined by Wilson *et al*. [29] as 'starvation' of the second medium. In other words, the effective absorption rate will be determined by the slowest layer 'upstream'. In this sense, the water uptake process in multi-layered materials may be understood as a unidirectional series circuit with specific conductive (permeability) properties for each layer and a certain hydraulic resistance associated with the interfaces between them [27].

The results of the capillary absorption tests for three-layer masonry composites, labelled M2 (2 interfaces), are shown in Figure 12 for the two studied configurations, namely B(a)-LMJ-B(b), and the opposite, B(b)-LMJ-B(a). Direct comparison of the water uptake mass is possible since the cross-sectional area of all the cylinders is the same. The location of the interfaces in the figure is estimated from the capillary saturation levels calculated from the capillary moisture content and the average volume of each material layer.

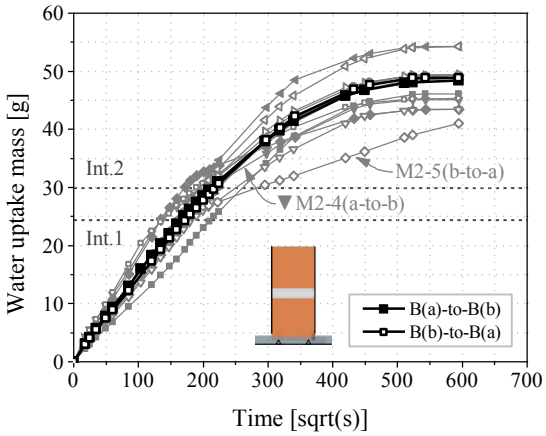

Figure 12. Water absorption results for masonry specimens M2 (B+LMJ+B). Grey curves represent test results and black curves are the corresponding average. The location of the interfaces is estimated from the average volume of each material layer.

The curves in Figure 12 reveal that the variability of the material response increases with the increasing number of elements involved. This is expected considering the more complex configuration of the specimens. Two main factors, namely variability of the brick layers and quality of the interfaces, give rise to the differences observed between the different specimens and the same specimens but in the opposite direction. The purpose of studying the same specimens in both directions is twofold. On one hand, the absorption properties of each brick layer may be assessed individually from the first portion of the water uptake curves. This helps to identify unavoidable variability from the bricks that could otherwise obscure the results. Secondly, a two-way analysis provides information about the directional nature of the interface. Indeed, if the interface is linked to a change in pore structure, it may become apparent when the flow goes from one material to the other but not the opposite. By testing the same components in the two directions, we were able to confirm the existence of such phenomenon.

As it was observed for the masonry specimens M1-M (Figure 11b), cases with slight, medium and high interfacial impact were detected as well for the three-layer composites (Figure 12). Most specimens showed hardly any absorption rate reduction between the first brick and the mortar joint. Only two cases, namely

M2-4(a-to-b) and M2-5(b-to-a) (individuated in Figure 12), presented a considerable absorption rate drop at the first interface, most probably associated with local defects. Conversely, a more noticeable deviation was generally observed between the mortar joint and the uppermost brick. This confirms the directional behavior of the interface and points at a microstructure change between B and LMJ. The pore quality difference between both materials is therefore assumed to be the main factor affecting the suction capacity of the following layer. In this case, the porous medium with finer pores tends to withhold water due to the higher capillary suction and thus the liquid transfer to a material with bigger pores is impeded.

Considering the average behavior of all the cases (black curves in Figure 12), the response of masonry specimens M2 showed no significant hydraulic resistance at the first interface (water moving from B to LMJ), whereas the second interface (water moving from LMJ to B) involved a certain flow reduction. Furthermore, the match between the averages of the two tested configurations proves that the behavior of the composite was independent of the analyzed direction.

3.2.2 Drying tests

The 1-D drying tests performed on two-layer (1 interface) masonry composites are analyzed in the following section. Figure 13 collects the results obtained for the two tested configurations, namely cylinders drying from the LMJ surface, labelled D1-M, and cylinders drying from the brick layer, labelled D1-B. The results are plotted as gravimetric moisture content with respect to the dry mass of the whole specimen (B+LMJ). For each case, the location of the interface is estimated from the capillary saturation level calculated from the capillary moisture content and the average volume of the exposed layer.

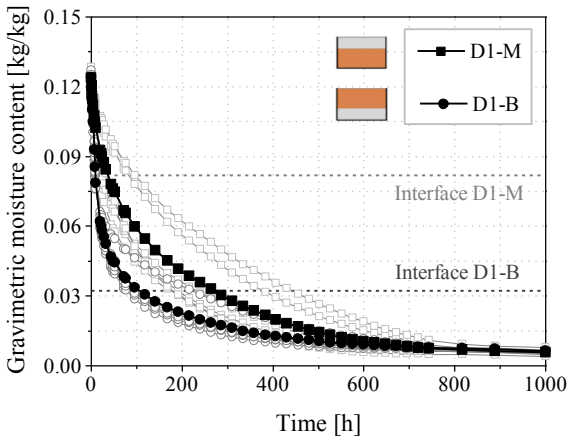

Figure 13. Drying test results for masonry specimens D1 (B+LMJ). Grey curves represent test results and black curves are the corresponding average. The location of the interfaces is estimated from the average volume of the exposed material layer.

The curves in Figure 13 show two distinct drying trends depending on the configuration of the composite. The specimens drying from the brick layer experienced a long initial phase (Stage I with linear mass loss) and a quite fast second stage. The same trend was observed for the drying tests of B and LM cubes (Figure 9, Figure 10). This response means that the stacked materials have the capacity to transport the liquid water effectively towards the surface where evaporation takes place. Conversely, the cylinders drying from LMJ showed a shorter initial drying phase and a prolonged, gradual second stage. This trend contrasts with the drying behavior of B and LM and is more related to the behavior of CM (Figure 9, Figure 10). Therefore, the LMJ on top rapidly exhausts its liquid transport capacity and then the drying behavior slows down considerably, shifting to vapor diffusion as the main transport mechanism for drying. This behavior may be explained by the presence of smaller pores in LMJ since finer pores withhold water due to their higher capillary pressure. Additionally, the presence of smaller pores is supported by the residual moisture content at the end of the experiments, which indicates the existence of a hygroscopic component, which was already anticipated by the sorption isotherms for LMJ (Figure 5d).

When comparing both cases, it is evident that the LMJ layer on top limits the drying rate of B below, which would be naturally faster as witnessed in the D1-B configuration. Considering the sharp front approximation to be extensible to drying processes, a receding drying front may be assumed [64]. Taking into account this receding moisture front, the existence of an interfacial resistance was expected to appear as a discontinuity in the mass loss curve, as it was observed for the water absorption cases in multi-layered compounds. Nonetheless, the mass loss figures reveal no clear influence of the interface. In general, the curves are smooth and no significant change is perceived beyond the transition from Stage I to Stage II. The effect of the mortar-brick interface in the drying process was also studied by Brocken [27] for brick-cement masonry specimens. Similarly, the author could not qualify the nature of the interface as having perfect or imperfect hydraulic contact.

Without further certainties about the role of the interface, we may assume a perfect hydraulic contact. In this scenario, two causes for the observed trends may be mentioned. On one hand, it seems conclusive that B has higher liquid transport capacity as well as higher vapor permeability. This would explain the longer Stage I and a considerably rapid Stage II for the configuration D1-B. Conversely, considering the D1-M cases, the liquid transport capacity of LMJ wears out quicker and a likely lower vapor permeability further limits the drying process of the brick layer behind. The low liquid permeability of LMJ observed in these drying tests contrasts with the absorption capacity of the same material observed in the previous water

uptake experiments. The disparity between absorption and drying confirms the hysteretic behavior observed in moisture storage for LMJ (Figure 5d).

4. CONCLUSIONS

An extensive experimental campaign was conducted to determine the hygric response of masonry materials. First, the hygric properties of constituent materials were assessed individually. Then, masonry was studied as a multi-layered composite material. The experimental program included vacuum saturation tests, static gravimetric tests for adsorption/desorption, dry/wet cup tests, capillary absorption tests, and 1-D isothermal drying. The hygric properties determined following the prescribed experimental procedures make up a consistent dataset and allow us to draw the following conclusions:

a) The results from the different experimental procedures are consistent and present acceptable variation. Nonetheless, vapor permeability measurements present poorer reliability, which has been documented by other authors as well, e.g. [16–18,54].

b) Extruded fired-clay bricks show a distinct anisotropic hygric behavior, more noticeable for faster processes such as water absorption. This behavior is explained by the existence of imperfections within the mass of the bricks derived from the extrusion process.

c) Differences are observed between the hygric response of the two studied molded mortars. This is most evident when comparing the moisture storage curves. LM shows low hygroscopicity and a strong capillary-active behavior with negligible hysteresis. Conversely, CM shows hygric activity in both the hygroscopic and capillary ranges with a marked hysteresis. Thus, the behavior of LM is much closer to that of the studied fired-clay brick.

d) The properties of the NHL-mortar prepared in molds differ from the same mixture cured in masonry bed joints. The discrepancies are associated with the different water-binder ratio resulting from water extraction by the bricks upon placement. The vacuum saturation tests on LMJ reveal lower open porosity and therefore lower saturation moisture content. The moisture storage curves obtained for LMJ show a more hygroscopic behavior than its molded counterpart, with non-negligible hysteresis. Water absorption tests performed on masonry cylinders M1-M show slower water uptake than expected from LM, thus a lower water absorption coefficient is assumed for LMJ. Furthermore, isothermal drying tests on masonry specimens drying from LMJ reveal mass loss curves with a short initial drying stage, which

is indicative of an enhanced water retention capacity and the presence of fine pores. Finally, the dissimilar trends observed for water uptake and drying processes confirm the hysteresis in moisture storage for LMJ.

e) In masonry specimens, the existence of an imperfect hydraulic contact at the brick-mortar interface is demonstrated for water absorption. The imperfect contact may be assumed as a hydraulic resistance and its effect varies from a slight reduction to considerable retardation of the water flow. The interfacial effect is mostly detected when the water movement goes from LMJ to B. Thus, discontinuity in the pore structure of the materials (finer pores in LMJ) is assumed as the main reason for the interfacial effect, which may become more pronounced due to the presence of local imperfections. The interfacial effect on drying kinetics is not evident.

f) Hygric properties obtained individually from testing the constituent materials separately cannot be directly extrapolated to multi-layered masonry cases. Two main phenomena must be taken into consideration in order to avoid erroneous estimations, namely: (a) for water absorption cases, there is a hydraulic interfacial resistance derived from the dissimilar pore structure between the materials in contact; (b) for water absorption and drying cases, the impact of curing conditions on the properties of mortars cast in masonry joints must be considered.

The current study provides a comprehensive insight into the hygric properties of masonry materials by relatively simple means. MIP results would be useful to confirm our conclusions related to the pore structure of the materials. Additionally, more complex methods, such as NMR, CT scan or X-Ray, could further improve our understanding since they provide moisture profiling inside the specimens. However, such techniques are costly and not always available. Provided that the sharp front approximation is applicable, the methodology presented in this paper provides all necessary data for a clear depiction of moisture transfer processes in multi-layered porous materials such as masonry.

Acknowledgements

The first author would like to thank his fellow PhD students at the University of Minho, in particular Meera Ramesh and Giorgos Karanikoloudis, for providing fundamental support with the experimental work.

Funding

This work was financed by national funds through FCT - Foundation for Science and Technology, under grant agreement SFRH/BD/117114/2016 attributed to the first author.

References

[1] M. Harrestrup, S. Svendsen, Full-scale test of an old heritage multi-storey building undergoing energy retrofitting with focus on internal insulation and moisture, Build. Environ. 85 (2015) 123–133. https://doi.org/10.1016/j.buildenv.2014.12.005.

[2] E. Vereecken, L. Van Gelder, H. Janssen, S. Roels, Interior insulation for wall retrofitting – A probabilistic analysis of energy savings and hygrothermal risks, Energy Build. 89 (2015) 231–244. https://doi.org/10.1016/j.enbuild.2014.12.031.

[3] M. van Aarle, H. Schellen, J. van Schijndel, Hygro-thermal simulation to predict the risk of frost damage in masonry – Effects of climate change, Energy Procedia. 78 (2015) 2536–2541. https://doi.org/10.1016/j.egypro.2015.11.268.

[4] F.M. Fernandes, Clay bricks, in: B. Ghiassi, P.B. Lourenço (Eds.), Long-Term Perform. Durab. Mason. Struct., Elsevier, 2019: pp. 3–19. https://doi.org/10.1016/B978-0-08-102110-1.00001-7.

[5] M. do Rosário Veiga, A. Santos Silva, Mortars, in: B. Ghiassi, P.B. Lourenço (Eds.), Long-Term Perform. Durab. Mason. Struct., Elsevier, 2019: pp. 169–208. https://doi.org/10.1016/B978-0-08-102110-1.00006-6.

[6] J.J. Brooks, Moisture Movement of Clay Brick Masonry, in: Concr. Mason. Movements, Elsevier, 2015: pp. 223–253. https://doi.org/10.1016/B978-0-12-801525-4.00008-X.

[7] M.S. Sciolti, M.A. Aiello, M. Frigione, Effect of thermo-hygrometric exposure on FRP, natural stone and their adhesive interface, Compos. Part B Eng. 80 (2015) 162–176. https://doi.org/10.1016/j.compositesb.2015.05.041.

[8] J.F. Straube, E.F.P. Burnett, Overview of Hygrothermal (HAM) Analysis Methods, in: H.R. Trechsel (Ed.), Moisture Anal. Condens. Control Build. Envel. – ASTM Man. Ser. MNL 40, American Society for Testing and Materials, Philadelphia, 2001: pp. 81–89.

[9] H.M. Künzel, A.N. Karagiozis, A.H. Holm, A Hygrothermal Design Tool for Architects and Engineers (WUFI ORNL/IBD), in: H.R. Trechsel (Ed.), Moisture Anal. Condens. Control Build. Envel. – ASTM Man. Ser. MNL 40, American Society for Testing and Materials, Philadelphia, 2001: pp. 136–151.

[10] H. Hens, Modeling the Heat, Air, and Moisture Response of Building Envelopes: What Material Properties are Needed, How Trustful Are the Predictions?, J. ASTM Int. 4 (2007) 1–11. https://doi.org/10.1520/JAI100460.

[11] G. Scheffler, Validation of hygrothermal material modelling under consideration of the hysteresis of moisture storage, Ph.D. dissertation, Dept. Civil Engineering, Dresden University of Technology, 2008.

[12] K. Kumaran, IEA Annex 24: Heat, Air and Moisture Transfer in Insulated Envelope Parts. Final Report, Volume 3, Taks 3: Material Properties, 1996.

[13] S. Roels, J. Carmeliet, H. Hens, O. Adan, H. Brocken, R. Czerny, C. Hall, A. Hamilton, K. Kumaran, Z. Pavlik, L. Pel, R. Plagge, F. Tariku, HAMSTAD Work Package 1: Final Report - Moisture Transfer Properties and Materials Characterisation, 2003.

[14] G. Cultrone, E. Sebastián, K. Elert, M.J. de la Torre, O. Cazalla, C. Rodriguez–Navarro, Influence of mineralogy and firing temperature on the porosity of bricks, J. Eur. Ceram. Soc. 24 (2004) 547–564. https://doi.org/10.1016/S0955-2219(03)00249-8.

[15] F.M. Fernandes, P.B. Lourenço, F. Castro, Ancient clay bricks: manufacture and properties, in: D.M. Bostenaru, R. Přikryl, A. Török (Eds.), Mater. Technol. Pract. Hist. Herit. Struct., Springer, 2010. https://doi.org/10.1007/978-90-481-2684-2.

[16] S. Roels, J. Carmeliet, H. Hens, O. Adan, H. Brocken, R. Cerny, Z. Pavlik, C. Hall, K. Kumaran, L. Pel, R. Plagge, Interlaboratory Comparison of Hygric Properties of Porous Building Materials, J. Therm. Envel. Build. Sci. 27 (2004) 307–325. https://doi.org/10.1177/1097196304042119.

[17] C. Feng, H. Janssen, Y. Feng, Q. Meng, Hygric properties of porous building materials: Analysis of measurement repeatability and reproducibility, Build. Environ. 85 (2015) 160–172. https://doi.org/10.1016/j.buildenv.2014.11.036.

[18] C. Feng, A.S. Guimarães, N. Ramos, L. Sun, D. Gawin, P. Konca, C. Hall, J. Zhao, H. Hirsch, J. Grunewald, M. Fredriksson, K.K. Hansen, Z. Pavlík, A. Hamilton, H. Janssen, Hygric properties of porous building materials (VI): A round robin campaign, Build. Environ. 185 (2020) 107242. https://doi.org/10.1016/j.buildenv.2020.107242.

[19] Y. Aït Oumeziane, A. Pierre, F. El Mankibi, V. Lepiller, M. Gasnier, P. Désévaux, Hygrothermal properties of an early 20th century clay brick from eastern France: Experimental characterization and numerical modelling, Constr. Build. Mater. 273 (2021) 121763. https://doi.org/10.1016/j.conbuildmat.2020.121763.

[20] R.J. Gummerson, C. Hall, W.D. Hoff, Water movement in porous building materials II. Hydraulic suction and sorptivity of brick and other masonry materials, Build. Environ. 15 (1980) 101–108. https://doi.org/10.1016/0360-1323(80)90015-3.

[21] K.J. Krakowiak, P.B. Lourenço, F.J. Ulm, Multitechnique Investigation of Extruded Clay Brick Microstructure, J. Am. Ceram. Soc. 94 (2011) 3012–3022. https://doi.org/10.1111/j.1551-2916.2011.04484.x.

[22] J.E. Lindqvist, K. van Balen, B. Bicer-Simsir, L. Binda, C. Bla¨uer, J. Elsen, E. Hansen, R. van Hees, F. Henriques, E.E. Toumbakari, T. von Konow, J.E. Lindqvist, P. Maurenbrecher, B. Middendorf, I. Papayanni, S. Simon, M. Subercaseaux, C. Tedeschi, M. Thompson, J. Valek, M.R. Valluzzi, Y. Vanhellemont, R. Veiga, A. Waldum, Rilem TC 203-RHM: Repair mortars for historic masonry. Testing of hardened mortars, a process of questioning and interpreting, Mater. Struct. 42 (2009) 853–865. https://doi.org/10.1617/s11527-008-9455-x.

[23] C. Groot, J. Gunneweg, The influence of materials characteristics and workmanship on rain penetration in historic fired clay brick masonry, Heron. 55 (2010) 141–154.

[24] C. Nunes, L. Pel, J. Kunecký, Z. Slížková, The influence of the pore structure on the moisture transport in lime plaster-brick systems as studied by NMR, Constr. Build. Mater. 142 (2017) 395–409. https://doi.org/10.1016/j.conbuildmat.2017.03.086.

[25] J.M.P.Q. Delgado, A.C. Azevedo, A.S. Guimarães, Drying Kinetics in Building Materials and Components: The Interface Influence, Springer, 2019. https://doi.org/10.1007/978-3-030-31860-4.

[26] K. Calle, T. De Kock, V. Cnudde, N. Van den Bossche, Liquid moisture transport in combined ceramic brick and natural hydraulic lime mortar samples: Does the hygric interface resistance dominate the moisture transport?, J. Build. Phys. 43 (2019) 208–228. https://doi.org/10.1177/1744259119857762.

[27] H.J.P. Brocken, Moisture transport in brick masonry: the grey area between bricks, Ph.D. dissertation, Dept. Built Environment, Technische Universiteit Eindhoven, 1998.

[28] M.A. Wilson, W.D. Hoff, C. Hall, Water movement in porous building materials—XIII. Absorption into a two-layer composite, Build. Environ. 30 (1995) 209–219.

[29] M.A. Wilson, W.D. Hoff, C. Hall, Water movement in porous building materials—XIV. Absorption into a two-layer composite (SA < SB), Build. Environ. 30 (1995) 221–227.

[30] C. Hall, W.D. Hoff, Water Transport in Brick, Stone and Concrete, 2nd ed., CRC Press, London, 2009.

[31] C. Groot, The characterisation of brick and mortar considering mortar/brick bond, in: M. Wu, Y. Qian (Eds.), Proc. 11th Int. Brick/Block Mason. Conf., ECS (Engineering Construction Standardization), Shanghai, 1997: pp. 50–58.

[32] C. Groot, J. Larbi, Influence of water flow (reversal) on bond strength development in young masonry, Heron. 44 (1999) 63–78.

[33] H. Derluyn, H. Janssen, J. Carmeliet, Influence of the nature of interfaces on the capillary transport in layered materials, Constr. Build. Mater. 25 (2011) 3685–3693. https://doi.org/10.1016/j.conbuildmat.2011.03.063.

[34] H. Janssen, H. Derluyn, J. Carmeliet, Moisture transfer through mortar joints: A sharp-front analysis, Cem. Concr. Res. 42 (2012) 1105–1112. https://doi.org/10.1016/j.cemconres.2012.05.004.

[35] X. Zhou, G. Desmarais, P. Vontobel, J. Carmeliet, D. Derome, Masonry brick–cement mortar interface resistance to water transport determined with neutron radiography and numerical modeling, J. Build. Phys. 44 (2020) 251–271. https://doi.org/10.1177/1744259120908967.

[36] BS EN 197-1:2011, Cement. Composition, specifications and conformity criteria for common

cements, (2011).

[37] BS EN ISO 12570:2000 + A1:2013, Hygrothermal performance of building materials and products - Determination of moisture content by drying at elevated temperature, (2000).

[38] C. Feng, H. Janssen, C. Wu, Y. Feng, Q. Meng, Validating various measures to accelerate the static gravimetric sorption isotherm determination, Build. Environ. 69 (2013) 64–71. https://doi.org/10.1016/j.buildenv.2013.08.005.

[39] RILEM TC 25-PEM, Recommended tests to measure the deterioration of stone and to assess the effectiveness of treatment methods (Test No. I.1 Porosity accessible to water), Matériaux Constr. 13 (1980) 176–179.

[40] BS EN ISO 12571:2013, Hygrothermal performance of building materials and products – Determination of hygroscopic sorption properties, (2013).

[41] M. Krus, Moisture Transport and Storage Coefficients of Porous Mineral Building Materials: Theoretical Principles and New Test Methods, Fraunhofer IRB Verlag, Stuttgart, 1996.

[42] ASTM E96/E96M-10, Standard Test Methods for Water Vapor Transmission of Materials, (2010). https://doi.org/10.1520/E0096.

[43] BS EN ISO 12572:2016, Hygrothermal performance of building materials and products – Determination of water vapour transmission properties – Cup method, (2016).

[44] EN 15803:2009, Conservation of cultural property - Test methods - Determination of water vapour permeability (δp), (2009).

[45] J.L. Monteith, M.. Shatleworth, Principles of Environmental Physics, 4th ed., Elsevier Ltd., London, 2013.

[46] BS EN ISO 15148:2002+A1:2016, Hygrothermal performance of building materials and products – Determination of water absorption coefficient by partial immersion, (2016).

[47] C. Feng, H. Janssen, Hygric properties of porous building materials (II): Analysis of temperature influence, Build. Environ. 99 (2016) 107–118. https://doi.org/10.1016/j.buildenv.2016.01.016.

[48] EN 16322:2013, Conservation of cultural property - Test methods - Determination of drying

properties, (2013).

[49] Z. Zhang, G. Scherer, Determination of water permeability for a moisture transport model with minimized batch effect, Constr. Build. Mater. 191 (2018) 193–205. https://doi.org/10.1016/j.conbuildmat.2018.09.194.

[50] H.M. Künzel, Simultaneous heat and moisture transport in building components: One- and two-dimensional calculation using simple parameters, Ph.D. dissertation, Dept. Building Physics, Fraunhofer Institute of Building Physics, 1995.

[51] Y. Mualem, A new model for predicting the hydraulic conductivity of unsaturated porous media, Water Resour. Res. 12 (1976) 593–622.

[52] S. Brunauer, P.H. Emmett, E. Teller, Adsorption of Gases in Multimolecular Layers, J. Am. Chem. Soc. 60 (1938) 309–319.

[53] M.T. van Genuchten, A closed form equation predicting the hydraulic conductivity of unsaturated soils, Soil Sci. Soc. Am. J. 44 (1980) 892–898.

[54] H. Hens, Applied Building Physics: Ambient Conditions, Building Performance and Material Properties, 2nd ed., Ernst & Sohn, Berlin, 2016. https://doi.org/10.1002/9783433607114.

[55] F. Descamps, Continuum and discrete modelling of isothermal water and air flow in porous media, Ph.D. dissertation, Building physics laboratory, KU Leuven, 1997.

[56] C. Groot, J. Gunneweg, Two views to deal with rain penetration problems in historic fired clay brick masonry, in: J. Válek, J.J. Hughes, C.J.W.P. Groot (Eds.), Proc. 2nd Conf. Hist. Mortars - HMC 2010 Final Work. RILEM TC 203-RHM, RILEM Publications SARL, Dordrecht, 2010: pp. 1005–1014.

[57] S. Roels, K. Vandersteen, J. Carmeliet, Measuring and simulating moisture uptake in a fractured porous medium, Adv. Water Resour. 26 (2003) 237–246. https://doi.org/10.1016/S0309-1708(02)00185-9.

[58] J. Carmeliet, J.-F. Delerue, K. Vandersteen, S. Roels, Three-dimensional liquid transport in concrete cracks, Int. J. Numer. Anal. Methods Geomech. 28 (2004) 671–687. https://doi.org/10.1002/nag.373.

[59] C. Feng, H. Janssen, Hygric properties of porous building materials (III): Impact factors and data processing methods of the capillary absorption test, Build. Environ. 134 (2018) 21–34. https://doi.org/10.1016/j.buildenv.2018.02.038.

[60] J. Selih, A. Sousa, T. Bremner, Moisture transport in initially fully saturated concrete during drying, Transp. Porous Media. 24 (1996) 81–106.

[61] M. Azenha, Numerical simulation of the structural behavior of concrete since its early ages, Ph.D. dissertation, Dept. Civil Engineering, University of Porto, 2009.

[62] C. Hall, W.D. Hoff, Rising damp: capillary rise dynamics in walls, Proc. R. Soc. A Math. Phys. Eng. Sci. 463 (2007) 1871–1884. https://doi.org/10.1098/rspa.2007.1855.

[63] E. Vereecken, P. Schůtová, S. Roels, How effective is kaolin clay for the creation of a perfect hydraulic interface contact between materials?, E3S Web Conf. 172 (2020) 14002. https://doi.org/10.1051/e3sconf/202017214002.

[64] L. Pel, H. Brocken, K. Kopinga, Determination of moisture diffusivity in porous media using moisture concentration profiles, Int. J. Heat Mass Transf. 39 (1996) 1273–1280.